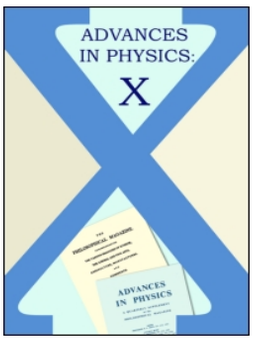

Advances in Physics: X

ISSN: (Print) 2374-6149 (Online) Journal homepage: http://www.tandfonline.com/loi/tapx20

Drop mobility on chemically heterogeneous and lubricant-impregnated surfaces

Giampaolo Mistura & Matteo Pierno

To cite this article: Giampaolo Mistura & Matteo Pierno (2017) Drop mobility on chemically heterogeneous and lubricant-impregnated surfaces, Advances in Physics: X, 2:3, 591-607, DOI: 10.1080/23746149.2017.1336940

To link to this article: http://dx.doi.org/10.1080/23746149.2017.1336940

Published online: 14 Jun 2017.

ADVANCES IN PHYSICS: X, 2017
VOL. 2, NO. 3, 591–607
https://doi.org/10.1080/23746149.2017.1336940

Taylor & Francis
Taylor & Francis Group

REVIEW ARTICLE

OPEN ACCESS Check for updates

Drop mobility on chemically heterogeneous and lubricant-impregnated surfaces

Giampaolo Mistura and Matteo Pierno

Dipartimento di Fisica e Astronomia "G. Galilei", Università di Padova, via Marzolo 8, 35131 Padova, Italy

ABSTRACT

Controlling the motion of liquid drops in contact with a solid surface has broad technological implications in many different areas ranging from textiles to microfluidics and heat exchangers. The wettability of a surface is determined by specifying the apparent contact angle and contact angle hysteresis (CAH) that depend on the surface chemistry and morphology. The presence of chemical inhomogeneity and morphological disorder usually increases CAH. A liquid substrate, whose surface is atomically flat and homogenous, is then expected to exhibit a very low CAH. Low CAH determines high drop mobility, while high CAH favours drop pinning. Very slippery surfaces with exceptional omniphobicity are obtained by impregnating a textured solid with a lubricant. To guide and control the motion of drops, the solid surface can be decorated with suitable chemical patterns. In this review, we briefly outline the main results obtained in the past few years to passively control drop motion and produce robust omniphobic surfaces, highlighting some of the most promising applications of these novel functional surfaces.

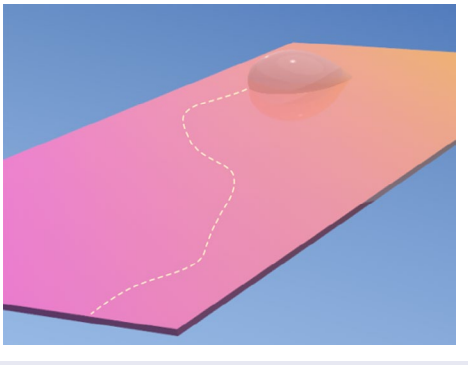

ARTICLE HISTORY
Received 13 March 2017
Accepted 25 May 2017

KEYWORDS
Wetting; drop mobility; contact angle hysteresis; liquid repellent surfaces; liquid-impregnated surfaces

PACS
68.08.Bc Wetting; 47.55.D- Drops and bubbles; 47.55.np Contact lines; 47.11.-j Computational methods in fluid dynamics

CONTACT Giampaolo Mistura giampaolo.mistura@unipd.it

1. Introduction

Controlling and predicting the mobility of drops in contact with a solid surface is a major scientific challenge, relevant for fundamental research [1] and crucial for an ample variety of applications including self-cleaning coatings [2], microfluidics [3], dropwise condensation [4] and fog collection [5]. The mobility of drops is deeply affected by substrate heterogeneities [6]. For instance, water drops can roll very easily, retaining a nearly perfect spherical shape on a surface that remains essentially dry, on various natural materials that include many plant leaves, bird feathers and fish skins [7], and artificial biomimetic surfaces produced in different ways [8]. By convention, these surfaces are called superhydrophobic if they exhibit a static apparent contact angle of the water drop with the surface exceeding 150°. Strong water repellence occurs because the roughness effectively increases the liquid–solid free energy [9]. This is the consequence of either a larger real contact area between the two components, the case of the liquid impregnating the surface (the so-called Wenzel state [2], Figure 1(a)) or a replacement of the true liquid–solid contact by a highly energetic liquid–vapour interface, the case of the liquid interface suspended on an air cushion on top of the roughness peaks (the so-called Cassie [2] or fakir state, Figure 1(b)). However, the dynamic behaviour of these two states is markedly different. For instance, Cassie drops like water drops on a lotus leaf roll off very easily even at inclinations well below 5°, removing dust particles present on the surface (self-cleaning or lotus effect [10]). Instead, partial impregnation of the surface texture by water causes strong

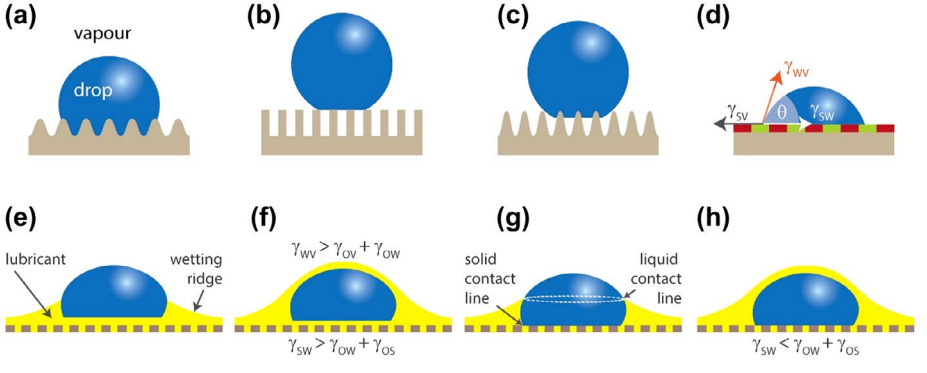

Figure 1. Schematic illustrations of possible wetting configurations of a textured surface (top) and of a slippery lubricant-impregnated surface (LIS) (bottom): (a) the liquid completely impregnates the grooves (Wenzel state); (b) the liquid is suspended on the asperities (Cassie state or lotus effect); (c) the liquid partially impregnates the texture (petal effect); (d) the liquid rests on a chemically heterogeneous surface forming an apparent contact angle θ described by Cassie equation; (e) and (g) the lubricant does not cloak the drop; (f) and (h) the lubricant cloaks the drop. Drops on LISs can exhibit zero (f), one (e) and (h) or two (g) three-phase contact lines.

Notes: The liquid contact line is the line at which the air, drop and lubricant meet, and the solid contact line is where the substrate, drop and lubricant meet. The interfacial tensions γ_{ij} between phases i and j are denoted as follows: γ_{ow} is the interfacial tension between the (water) drop and the lubricant oil; γ_{sw} the interfacial tension between the surface and the drop; γ_{so} the interfacial tension between the surface and the lubricant. γ_{wv} represents the surface tension drop–vapour (air) and γ_{ov} the surface tension oil–vapour (air) (Figure freely adapted from [8,13]).

pinning of the drops (petal effect [11], Figure 1(c)). Design-wise, imparting superhydrophobicity to a surface is not a difficult task. However, attaining robustness of the material over time and/or under external constraints has proved challenging [9]. For instance, the air cushions required to sustain Cassie drops can be collapsed by a variety of external factors like wetting pressures, can diffuse away into the surrounding liquid, can lose robustness upon damage to the texture and may be displaced by low surface tension liquids unless a special texture design is implemented [12].

A different approach to achieve non-wetting properties involves surfaces containing pockets of a lubricating liquid rather than of air [14,15]. These novel functional surfaces, known as liquid-infused surfaces (LIS) [14], lubricant-impregnated surfaces (LIS) [12] or slippery liquid-infused porous surfaces (SLIPS) [15] (in the following identified with the acronym LIS), are textured materials usually imbibed by a lyophilic oil as shown in the bottom illustrations of Figure 1. The premise for such a design is that a liquid surface is intrinsically smooth and defect-free down to the molecular scale; provides immediate self-repair by wicking into damaged sites in the underlying substrate; is largely incompressible; and can be chosen to repel immiscible liquids of virtually any surface tension [15]. A drop of a liquid, which is immiscible and energetically unfavourable with the substrate compared with the lubricant, can slide on a LIS very easily as shown in the examples of Figure 2. This feature has already been exploited in a series of interesting applications. However, the lack of pinning sites makes very difficult to control the motion of drops on LISs. Suitable chemical patterning of surfaces provides a viable route to overcome these limitations.

To model and simulate the sliding of droplets on these surfaces, different approaches might be followed [1,16–21]. Assuming the fluids as a continuum, one can solve the Navier–Stokes equation describing the evolution of the full velocity field complemented with appropriate boundary conditions at the solid–liquid and the liquid–air interfaces [18]. Alternatively, one may combine the bulk equations with an additional phase-field dynamics, thereby modelling the liquid–air interface as diffuse [22,23]. More fundamental approaches are particle-based discrete methods, such as molecular dynamics [19]. These methods are capable of simulating phenomena where the continuum assumption breaks down. On the other hand, they require a prohibitively large computational effort and thus are restricted to nanodroplets [18]. Finally, the lattice Boltzmann (LB) method is a mesoscopic approach based on the kinetic theory expressed by the original Boltzmann equation [20]. The scale-bridging nature of the LB method is a fundamental advantage, which allows it to incorporate the essential microscopic or mesoscopic physics while recovering the macroscopic laws and properties at affordable computational cost.

In this review, we briefly outline the main results obtained in the past couple of years to passively guide drops and produce robust omniphobic surfaces, highlighting some of the most relevant applications of these novel functional surfaces.

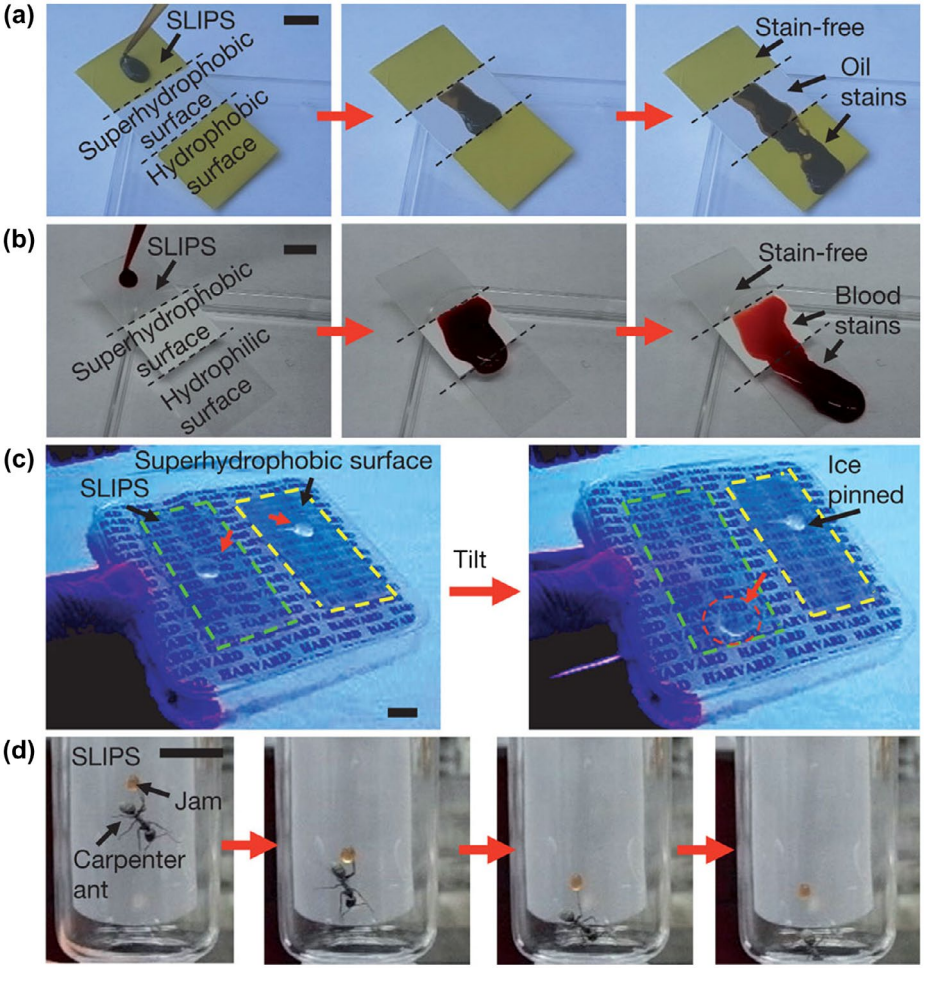

Figure 2. Repellence of complex fluids, ice and insects by SLIPS. (a) Movement of oil on a SLIPS, a superhydrophobic Teflon porous membrane and a flat hydrophobic surface. Note the slow movement on and staining of the latter two regions. (b) Comparison of the ability to repel blood by a SLIPS, a superhydrophobic Teflon porous membrane and a flat hydrophilic glass surface. Note the slow movement on and staining of the latter two regions. (c) Ice mobility on a SLIPS (highlighted in green) compared to strong adhesion to an epoxy resin-based nanostructured superhydrophobic surface (highlighted in yellow). (d) Demonstration of the inability of a carpenter ant to hold on to SLIPS. The ant (and a drop of fruit jam it is attracted to) slide along the SLIPS when the surface is tilted.

Notes: Note that the ant can stably attach to normal flat hydrophobic surfaces, such as Teflon. All scale bars represent 10 mm. Reproduced with permission from Ref. [15]. Copyright 2011, Macmillan Publishers Limited.

2. Drops on chemically heterogeneous surfaces

2.1. Basic principles

The possibility of using chemically heterogeneous surfaces (CHS) to guide wetting drops along certain directions has recently attracted much attention both theoretically [24–32] and experimentally [33–38]. In these studies, the driving force is provided by the down-plane component of the drop weight $F_g = \rho V g \sin\alpha$, acting on

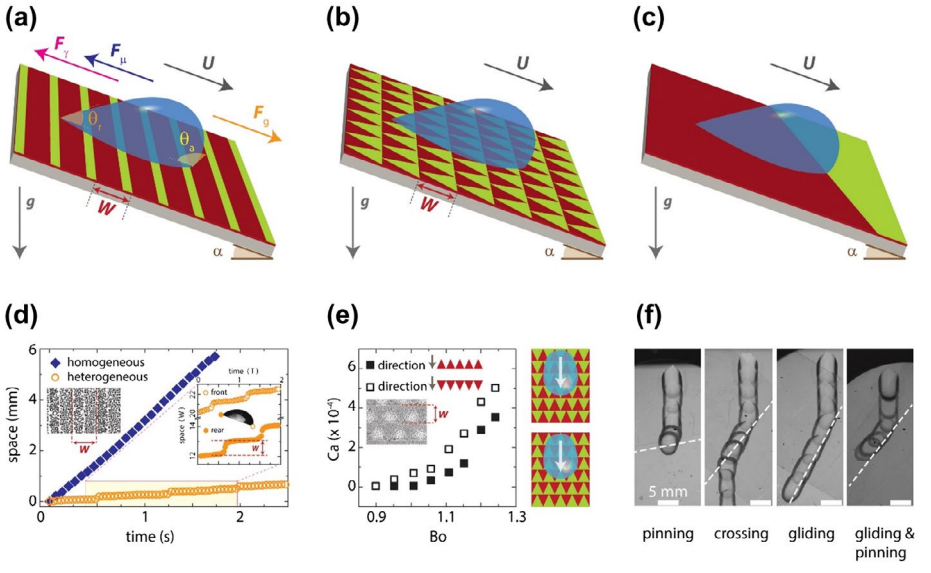

Figure 3. (a) Sliding of a liquid drop of volume V on a plane tilted by an angle α. The liquid has density ρ and viscosity μ. The sliding velocity U is the result of the balance between the down-plane component of the gravitational force $F_g = \rho V g \sin\alpha$, the interfacial force $F_\gamma \sim \gamma_{wv} V^{1/3}(\cos\theta_A - \cos\theta_R)$ and the viscous force $F_\mu \sim \mu U V^{1/3}$ [28]. The advancing contact angle θ_A is larger than the receding angle θ_R. The surfaces may be functionalized with stripes of alternating wettability with periodicity W. (b) Red triangular domains represent (glass) hydrophilic parts, and green areas symbolize (OTS) hydrophobic regions. (c) Chemical step formed between a hydrophilic and a hydrophobic region. (d) Time evolution of the drop frontal point on homogeneous and striped (shown in the accompanying condensing figure) surfaces presenting the same static contact angle. The enlargement shows the characteristic stick-slip behaviour for both the front and rear contact points of the sliding drop. (e) Ca number (e.g. mean velocity) as a function of Bo number (e.g. plane inclination α) on the triangular patterns indicating that drops slide down faster along the direction ▼↓ Red Down-pointing triangle: character code 25Bc from Unicode (hex), up to 50% with respect to the opposite direction ▲↓ Red Up-pointing triangle: character code 25B2 from Unicode (hex), respectively. (f) Sequence of the four possible trajectories exhibited by a drop approaching a chemical step: (a) the drop pins; (b) the drop crosses the step; (c) the drop glides along the step; and (d) the drop partially glides along the step and pins at a later stage.

Note: Figure freely adapted from [30,37,38].

a drop of volume V and density ρ sliding down an inclined plane tilted by an angle α (see Figure 3). It is balanced by the interfacial force $F_\gamma = kw\gamma_{wv}(\cos\theta_A - \cos\theta_R)$ [39] where k is a constant that depends on the drop shape, $w \sim V^{1/3}$ is the width of the drop, γ_{wv} the surface tension between liquid (water) and vapour (air) and $(\Delta\theta = \theta_A - \theta_R)$ is the contact angle hysteresis CAH, with θ_A and θ_R the advancing and receding contact angles, respectively, schematically indicated in Figure 3(a). CAH is the key macroscopic parameter governing drop dynamics. Drops move spontaneously on surfaces that exhibit no CAH, even if the contact angles are very small. Otherwise, the incline must be tilted above a certain critical angle α_c for drops to start sliding because of gravity. In a situation governed by the no-slip boundary condition of fluid mechanics (most situations), droplet movement

is controlled by kinetics and not thermodynamics, and the activation barrier depends only on the structure of the three-phase contact line, which is a 1D issue. The contact line can be destabilized, eliminating hysteresis, through surface morphology control which increases the length, discontinuity, and tortuosity of the contact line, and decreases the energy difference between metastable states [39,40].

The presence of domains of different wettability on a flat surface favours instead the pinning of the contact line at the domain contour [1,6]. Actually, when drops are deposited on a surface functionalized with stripes of alternating wettability, they may assume elongated shapes, which are characterized by different contact angles in the directions perpendicular and parallel to the stripes. Such a morphological anisotropy induced by lateral pinning on CHS has been the object of intense scrutiny in a variety of situations [41–44] and can be exploited to create droplets with a tailored three-dimensional geometry at the macro and microscales on different hydrophilic regions [45] or to spatially control the heterogeneous nucleation of water on hydrophilic stripes alternated by hydrophobic stripes that exhibit a significant contrast in their intrinsic wettability [46].

The motion of sliding drops is also hampered by viscous forces. For small drops, bulk dissipation is usually smaller than the dissipation close to the contact line [47] and the viscous drag depends linearly on the drop velocity U and the viscosity of the liquid μ. As a result, the sliding of drops down an inclined, chemically homogeneous surface occurs at a constant speed, whose value increases with the tilt angle α and drop volume V and depends on the surface wettability: the larger the apparent contact angle, the higher U [21,28,37,48–50].

2.2. Stick-slip motion on CHS

Patterning the surface with alternating stripes of sub-millimetric width and different wettability introduces an anisotropic behaviour: drops slide more easily along the alternating stripes than across them [33,51] and periodic variations in the contact angles, possibly accompanied by fluctuations in the drop velocity, take place along this latter direction [33].

More interestingly, if the wettability contrast between adjacent stripes is high enough, drops undergo a stick-slip motion whose average speed can be an order of magnitude smaller than that measured on a homogeneous surface having the same apparent contact angle [37] as displayed in Figure 3(d). This motion is the result of the periodic deformations of the drop interface when crossing the stripes. Lattice Boltzmann simulations reproduce the stick-slip motion and indicate that the slowdown is the result of the pinning–depinning transition of the contact line, which causes energy dissipation to be localized in time and a large part of the driving energy to be stored in the periodic deformations of the contact line when crossing the stripes [28,37]. A stick-slip dynamics is also observed during drop evaporation [52–55] and drop impingement and spreading [56] on CHS patterned with hydrophobic and hydrophilic stripes. More generally, CHS

formed by domains of different shapes printed on flat substrates and arranged in various patterns strongly affect both the statics (e.g. the sliding angle) and the dynamics (e.g. the average speed) of moving drops [34,36,38]. In particular, on the triangular domains, anisotropic behaviour is found with drops sliding down faster when the tips of the hydrophilic triangles are pointing in the down-plane direction [38] as shown in Figure 3(e). Chemically heterogeneous patterns also influence the morphology and dynamics of pendant drops [57].

2.3. Passive control of drop motion on CHS

When a gravity-driven water drop impinges on a chemical step formed at the junction between a hydrophilic and a hydrophobic region at a finite tilt angle, the presence of the step breaks the reflection symmetry of the drop shape while the induced deformation creates a coupling of the drop mobility into parallel and perpendicular directions [30]. Such a 'cross-talk' would be hindered if the surfaces had a contrast in surface energy but vanishing contact angle hysteresis. A rich spectrum of dynamic regimes is observed: pinning at the step, crossing of the step, gliding along the step and gliding along the step for a short distance, followed by pinning at the step as displayed in Figure 3(f). Trapping of a liquid drop by a wetting defect represented by a hydrophilic stripe is controlled by two dimensionless parameters, the trapping strength measured in units of the driving force and the ratio between a viscous and an inertial timescale [58]. For highly viscous liquids, the drop stops when the trapping strength is equal to the gravitational driving force. Instead, for weakly viscous liquids, inertia dominates over viscous dissipation, e.g. the viscous timescale is higher than the inertial one, and increasingly deeper defects are required to trap the drops.

These findings suggest workable strategies to passively control the motion of drops by a suitable tailoring of the chemical pattern which can find applications in different areas. For instance, nanolitre-sized droplets can be effectively manipulated on hydrophilic/superhydrophobic patterned surfaces that present high contrast of wettability and adhesion [59–62]. Depositing drops on such hybrid surfaces results in a parallel process where multiple different liquids can be deposited simultaneously with a high throughput (see Figure 4(i)) [59]. Patterning superhydrophobic titania nanotube array by site-selective alcohol-based ink [61] or superhydrophobic paper with black ink [62] produces drops tacking guides of variable shape (see Figure 4(ii)). Pumpless transport of liquid at high flow rates on open microfluidic platforms can be achieved with a substrate-independent, wettability patterning method [63]. Wedge-shaped superhydrophilic planar tracks laid on a hydrophobic background are the building blocks of these devices. Liquid dispensed at the narrow ends of a superhydrophilic wedge track gets transported to the wider ends by hemiwicking and Laplace pressure-driven flows (see Figure 4(iii)). CHS can be used to tune the spatial distribution of supercooled condensation and subsequently control the geometry and speed of inter-droplet frost growth, providing a method

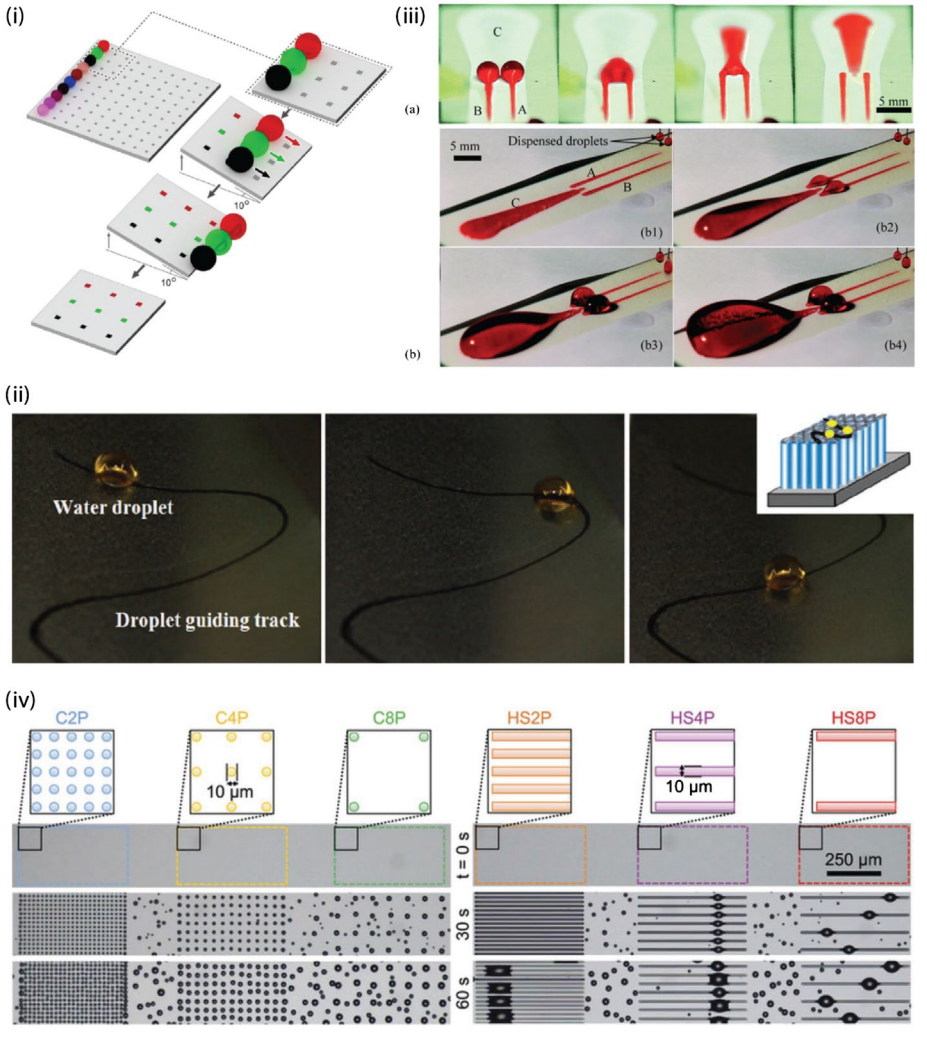

Figure 4. Passive control of drop motion on CHS. (i) Deposition by sliding drops on patterned CHS: (left figure) different kinds of liquids are placed on the first row of a 10 × 10 matrix of hydrophilic pads surrounded by superhydrophobic substrate; (right figures) zoomed view of sliding drops deposition process [59]. (ii) Sequential pictures of a water drop moving along a well-defined track obtained by site-selective alcohol-based ink patterning of titania nanotube array [61]. (iii) Pumpless functional surface devices capable of performing liquid bridging and draining. (a) Elevated end view sequence displaying liquid bridging and draining on a horizontal paper substrate. (b) Collection of liquid on the bridge circuit on a horizontal transparency (PET) film substrate after pumping for (b1) 1 cycle (~56 μL), (b2) 4 cycles (~226 μL), (b3) 7 cycles (~395 μL) and (b4) 10 cycles (~564 μL). The liquid (water) is dyed for better visualization [63]. (iv) Spatial control of condensation on smooth CHS composed of arrays of circles or stripes effective in preventing the in-plane growth of ice.

Notes: The coloured shapes in the schematics represent the hydrophilic features while the white background is hydrophobic. Time zero corresponds to the onset of cooling from 10 °C down to a steady-state temperature of −10 °C from 30 s onward [64]. Reproduced with permission from Refs. [59,61,63,64]. Copyright 2016 AIP Publishing, 2013 John Wiley and Sons, Inc., 2014 The Royal Society of Chemistry, 2016 Macmillan Publishers Limited.

to passively prevent the in-plane growth of ice (see Figure 4(iv)) [64]. They can also significantly enhance the pool boiling performance [65]: the best improvement arises with hydrophilic surfaces featuring hydrophobic islands, which efficiently prevent the formation of an insulating vapour layer. Finally, heterogeneous wettability of the channel wall can alter the stability and dynamics of oil-in-water emulsions generated in a microfluidic device [66]. Patterning the wall of a glass capillary with alternating hydrophilic and hydrophobic regions introduces a universal critical timescale, above which the microfluidic emulsions remain stable and intact, whereas below they become adhesive or inverse.

3. Drops on lubricant-impregnated surfaces

3.1. Basic principles

Effective strategies to produce very slippery surfaces that hardly pin sessile drops consist in trapping a lubricating liquid inside a texture, and choose this liquid for allowing a drop of another liquid to float on this mixed substrate [14,15]. A new class of materials is thus defined, which are hemi-liquid and hemi-solid, where the liquid phase is trapped by the solid cavities. This approach is inspired by systems such as the Nepenthes pitcher plant that use them to lock-in an intermediary liquid that then acts as the repellent surface [67]. In pitcher plants, this liquid film is aqueous and effective enough to cause insects that step on it to slide from the rim into the digestive juices at the bottom by repelling the oils on their feet [68]. In the laboratory, an ample variety of synthetic substrates has been used to trap the lubricant, including Teflon nanofibrous membranes [15], hierarchical textures comprising microposts covered with nanofeatures fabricated using laser ablation [69], regular arrays of microposts of different shape [70] and parallel grooves [71] made by standard photolithographic techniques, nanostructured coatings made by electrodeposition of highly textured polypyrrole on Al substrates followed by fluorination of the structured coating [72], porous polymeric films synthesized on glass [73], silicone oil films deposited on a substrate and annealed at high temperature [74], flexible nanocellulose films by photoinduced thiolne functionalization [75], sol–gel-derived nanocomposite coatings [76] and self-assembly polystyrene microbeads on scotch tapes with the aid of an inkjet printer [77]. As infused lubricants, silicone oils of different degrees of viscosity, fluorinated oils of very low surface tension and low volatile ionic liquids are commonly used.

Since a drop on a LIS comprises four distinct phases (the textured solid, the lubricant, the liquid that needs to be shed and the surrounding gas,), it exhibits a quite rich phenomenology. Actually, there exist 12 different thermodynamically stable wetting states depending on the interfacial tensions, the roughness and the solid fraction [12]. The most relevant configurations favouring slippery behaviour, i.e. configurations where the drop does not wet the substrate, are schematically represented in the bottom snapshots of Figure 1 [13]. The drop may rest on top of the lubricant (Figure 1(e) and (f)), it may sink into the lubricant and rest on

top of the protrusions (Figure 1(g) and (h)) or it may penetrate into the textured substrate, thereby replacing the lubricant (not shown). Either the lubricant cloaks the drop (Figure 1(f) and (h)) or the drop sinks into the lubricant up to a certain height, at which point the lubricant forms an annular wetting ridge around the drop that is pulled above the substrate (Figure 1(e) and (g)). Depending on the interplay of the interfacial tensions, a LIS can exhibit zero (Figure 1(f)), one (Figure 1(e) and (h)) or two (Figure 1(g)) three-phase contact lines.

Stable impregnation requires the contact angle θ_{os}(v) of the impregnating oil (subscript 'o') on the smooth solid (subscript 's') in the presence of vapour (labelled as 'v') to be less than a critical angle θ_c, given by the expression $\theta_c = \cos^{-1}\frac{1-\phi}{r-\phi}$, where ϕ is the fraction of the projected area of the surface that is occupied by the solid and r is the roughness of the substrate [14]. The submergence or exposure of texture tops under the droplet is dictated by the spreading coefficient of the impregnating oil on the solid in the presence of the drop given by $S_{os}(w) = \gamma_{sw} - \gamma_{ow} - \gamma_{os}$, where γ_{ij} is the interfacial energy between the phases i and j. In the case of complete spreading of the lubricant on the surface ($S_{os}(w) > 0$), a thin van der Waals film submerges the top of textures and weakens or even eliminates pinning sites [12]. In addition to the above two conditions, it is important to consider the possibility of cloaking (or encapsulation) of drops by the impregnated oil because it may prevent condensate growth, accelerate oil depletion from the texture and contaminate the droplets [70]. This can happen when the spreading coefficient of oil on water in the presence of vapour is positive, i.e. $S_{ow}(v) = \gamma_{wv} - \gamma_{ov} - \gamma_{ow} > 0$. Conversely, the liquid may completely spread on oil if $S_{wo}(v) = \gamma_{ov} - \gamma_{wv} - \gamma_{ow} > 0$. In the case of water drops, cloaking occurs with silicone or fluorinated oils as lubricants, whereas no cloaking takes place with ionic liquids. Furthermore, the lubricating film also serves as a self-healing coating to rapidly restore the liquid-repellent function following damage of the porous material by abrasion or impact [15,78].

While thermodynamics arguments are sufficient to predict the presence of different drop configurations on LIS, to date there is no theory for computing the corresponding values of the contact angle and contact angle hysteresis, despite their relevance as key design parameters for any application. To further complicate matters, the apparent contact angle is not uniquely defined by material parameters, but has a dependence on the relative size between the droplet and its surrounding wetting ridge formed by the infusing liquid [79]. To better understand the interface characteristics of such systems, the dynamics of a pendant water drop in air that contacts a substrate coated by thin oil films is studied at different timescales. At short times, the water drop is deformed by the oil that spreads onto the water–air interface, and the dynamics are characterized by inertial and viscous regimes. At late times, the oil film under the drop relaxes either to a stable thin film or ruptures [80].

3.2. Drop motion on weak pinning LIS

As expected, the dynamics of drops on inclined LIS is likewise quite rich [12]. Encapsulated drops with no contact lines on the textured substrate start to move

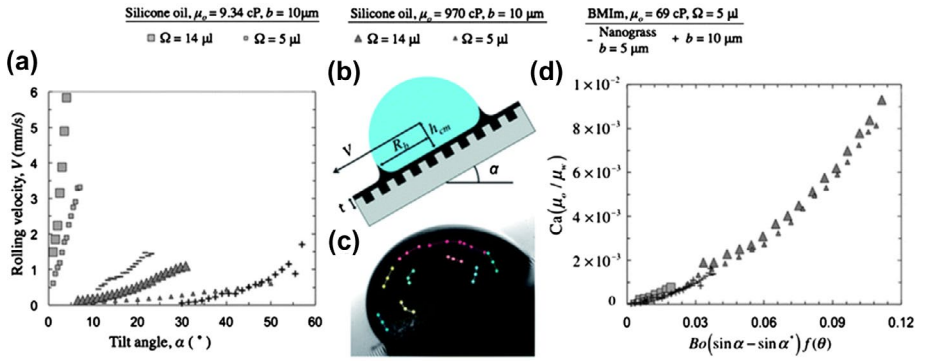

Figure 5. (a) Measured velocities of water droplets as a function of substrate tilt angle for various lubricant viscosities, post spacings and droplet sizes. (b) Schematic of a water droplet moving on a lubricant-impregnated surface showing the various parameters considered in the scaling model. (c) Trajectories of a number of coffee particles measured relative to the water droplet reveal that the drop rolls rather than slips across the surface. (d) Non-dimensional plot from the model collapses the data-sets shown in (a) onto a single curve indicating that the model captures the main physics of the problem.
Notes: Reproduced with permission from Ref. [12]. Copyright 2013, The Royal Society of Chemistry.

at very small inclination angles of just a few degrees regardless of the post spacing and oil viscosity. On the other hand, drops in direct contact with emergent post tops show much higher roll-off angles that are strongly texture dependent. In analogy to drops sliding down CHS, the speed of drops on an inclined LIS increases with the substrate tilt angle α and drop volume V and decreases with ϕ as reported in Figure 5. However, drops on a LIS are found to roll rather than slide with velocities that vary inversely with lubricant viscosity. The experimental data nicely satisfy a scaling model derived from the assumption that the gravitational potential energy of the rolling drop is primarily consumed in viscous dissipation in the wetting ridge around the base of the rolling drop [12].

3.3. Applications of weak pinning LIS

The extremely weak pinning of LISs makes these functional surfaces ideal for a variety of important applications. For instance, LISs enhance water transportation by means of temperature gradients. Using a lubricant with viscosity comparable to that of water and temperature gradients as low as 2 K/mm, drops can propel at 6.5 mm/s [69], that is at least five times quicker than reported on conventional substrates [81,82]. In addition, the apparent contact angle on LISs is typically around 90°, that is low enough to provide significant contact with the substrate and thus significant temperature differences between both edges of the deposited droplet, unlike what is observed on superhydrophobic surfaces for which contact is minimized. Condensation of water drops on a LIS occurs with enhanced droplet mobility compared to superhydrophobic surfaces. The enhancement results from the fact that the condensed droplets stay afloat on

the lubricant with minimal pinning to the surface compared with superhydrophobic surfaces, where droplets grow within textures and get strongly pinned. Since the condensation heat transfer is a strong function of droplet mobility, it is expected that surfaces impregnated with ionic liquids or other lubricants that avoid cloaking exhibit superior heat transfer performance [70]. Furthermore, LISs can be icephobic [83,84]. A scalable and reproducible coating method has been developed to fabricate a LIS coating on aluminium, one of the most widely used lightweight structural materials [72]. The resulting surface not only significantly reduces ice accumulation by allowing the condensed water droplets to slide off before they freeze but also enable the easy removal of the accumulated ice and melted water by gravity at low tilt angles. The highly reduced ice adhesion strength measured on LIS-Al (~15 kPa, 1–2 orders of magnitude smaller compared to conventional materials) presents a great opportunity to utilize LIS-based icephobic surfaces for broad applications in the refrigeration and aviation industry, as well as in other high-humidity environments working at low temperatures [72,85]. Finally, LISs are promising candidates for anti-biofouling coatings, alternative to common methods based on toxic release, intensive chemical attack or mechanical removal [86,87]. Bacteria primarily exist in robust, surface-associated communities known as biofilms, ubiquitous in both natural and anthropogenic environments. Mature biofilms resist a wide range of antimicrobial treatments and pose persistent pathogenic threats. A reduction in biofilm attachment over a seven-day period of up to 96–99.6% is reported for some of the most common and opportunistic pathogens in both terrestrial and aquatic environments [86], an improvement of more than one order of magnitude vs. best-case scenario PEG-functionalized surfaces [88]. This easily implementable technology provides a promising approach to substantially reduce the risk of device infection and associated patient morbidity [89] and biocompatible coatings on medical devices to prevent thrombosis [90] or improve operative field visibility in endoscopy [91]. Slippery LISs show also good repellency against marine macrofouling organisms [73,92].

A systematic demonstration of drag reduction using LIS for a variety of lubricant to working liquid viscosity ratios is provided by cone and plate rheometry [93]. Consistent with theory, little or no drag reduction is observed for working liquids with a viscosity μ_w around that of the lubricant ($\mu_w < 30\mu_o$). As the working liquid becomes more viscous ($\mu_w > 100\mu_o$), drag reduction is observed. With the most viscous working liquid ($\mu_w = 210\mu_o$), a drag reduction of 16% is observed, which correlates to a slip length of 18 μm. However, when these surfaces are immersed in dynamic fluid environments, external flow can shear away the impregnated liquid layer that is responsible for their advantageous properties. While some of the impregnated liquid drains for both gravity and shear-driven failure, a finite length of the surface remains impregnated indefinitely under a constant external forcing [71]. In both cases, if the impregnated region of a surface is longer than the retainable length, the liquid that is above or upstream of the stable region will

drain. In the case of LIS with longitudinal grooves, an analytical expression for the persistence length is obtained by considering both the shear stress and the external pressure gradient [94]. It shows that a higher shear stress or external pressure gradient results in lower lubricant retention and, for a given external fluid and a fixed shear stress, the less viscous lubricants achieve higher retention. A method to prevent drainage from textured surfaces consists in creating sacrificial regions with differing chemistry or using a lower lubricant viscosity [95].

4. Conclusions and perspectives

In this concise review, there is of course neither space nor scope for dozens of exciting ongoing research lines on functional surfaces exhibiting unusual wetting behaviours. Yet, we hope to have given at least the flavour of some new and interesting strategies to passively control the direction of sessile drops by exploiting the pinning barriers exerted by suitable lyophilic/lyophobic patterns printed on a surface and to obtain strong omniphobicity because of the weak pinning arising from the presence of a liquid substrate. These aspects can be synergistically combined to produce new functional surfaces which provide unprecedented droplet growth and transport by mimicking specific mechanisms of different living systems [4].

The very recent results highlighted in this review suggest that the research of new, effective ways to control drop mobility on surfaces will blossom in the coming years and will find interesting application in different areas. For instance, by infusing lubricants in porous matrices, a new class of adaptive materials can be conceived that enable a single surface to reversibly span an entire range of functional properties from one extreme to the other, with stimulus-sensitive tunability. A good example of the functions that can be realized exploiting adaptive materials obtained by infusing with a lubricant a Teflon membrane glued to an elastic polydimethylsiloxane film is the ability to simultaneously adjust the surface's transparency and reversibly start and stop the sliding of the oil droplets by the application of a graded mechanical stimulus [96].

A promising alternative to electrowetting [97] to achieve active control of the drop motion relies on the use ferrofluids in the presence of external magnetic fields [98–105]. Ferrofluids along with a magnetic field that locks them in place form magnetic slippery surfaces with no required micro/nano fabrication more icephobic than standard LIS [106]. Water drops deposited on these liquid magnetic surfaces move at very low tilt angles with little friction. More generally, it will be possible to integrate passive control provided by CHS with the action exerted by magnetic fields.

Apart from these fascinating applications, a key aspect that remains to be addressed for the engineering/commercialization of devices based on these functional surfaces is their stability over time after prolonged exposure to air, light, pressure and other physicochemical agents.

Acknowledgements

Discussions and collaborations with F. Ancilotto, M. Brinkmann, C. M. Casciola, E. Chiarello, G.L.W. Cross, L. Derzsi, D. Ferraro, D. Filippi, G. Fois, L. Persano, D. Pisignano, C. Rigoni, C. Sada, P. Sartori, C. Semprebon, T. Tóth, S. Varagnolo and, in particular, M. Sbragaglia are gratefully acknowledged.

Disclosure statement

No potential conflict of interest was reported by the authors.

ORCID


Giampaolo Mistura http://orcid.org/0000-0002-3426-5475

References

[1] D. Bonn, J. Eggers, J. Indekeu, J. Meunier and E. Rolley, Rev. Mod. Phys. 81 (2009) p.739.
[2] D. Quéré, Annu. Rev. Mater. Res. 38 (2008) p.71.
[3] R. Seemann, M. Brinkmann, T. Pfohl and S. Herminghaus, Rep. Prog. Phys. 75 (2012) p.016601.
[4] K.C. Park, P. Kim, A. Grinthal, N. He, D. Fox, J.C. Weaver and J. Aizenberg, Nature 531 (2016) p.78.
[5] F.T. Malik, R.M. Clement, D.T. Gethin, W. Krawszik and A.R. Parker, Bioinspir. Biomim. 9 (2014) p.031002.
[6] P.G. de Gennes, F. Brochard-Wyart and D. Quéré, *Capillarity and Wetting Phenomena: Drops, Bubbles, Pearls, Waves*, Springer, New York, 2004.
[7] S. Nishimoto and B. Bhushan, RSC Adv. 3 (2013) p.671.
[8] P. Roach, N.J. Shirtcliffe and M.I. Newton, Soft Matter 4 (2008) p.224.
[9] L. Bocquet and E. Lauga, Nat. Mater. 10 (2011) p.334.
[10] W. Barthlott and C. Neinhuis, Planta 202 (1997) p.1.
[11] L. Feng, Y. Zhang, J. Xi, Y. Zhu, N. Wang, F. Xia and L. Jiang, Langmuir 24 (2008) p.4114.
[12] J.D. Smith, R. Dhiman, S. Anand, E. Reza-Garduno, R.E. Cohen, G.H. McKinley and K.K. Varanasi, Soft Matter 9 (2013) p.1772.
[13] F. Schellenberger, J. Xie, N. Encinas, A. Hardy, M. Klapper, P. Papadopoulos, H.J. Butt and D. Vollmer, Soft Matter 11 (2015) p.7617.
[14] A. Lafuma and D. Quéré, EPL 96 (2011) p.56001.
[15] T.-S. Wong, S.H. Kang, S.K.Y. Tang, E.J. Smythe, B.D. Hatton, A. Grinthal and J. Aizenberg, Nature 477 (2011) p.443.
[16] V. Cristini and Y.C. Tan, Lab Chip 4 (2004) p.257.
[17] J.H. Snoeijer and B. Andreotti, Annu. Rev. Fluid Mech. 45 (2013) p.269.
[18] Y. Sui, H. Ding and P.D.M. Spelt, Annu. Rev. Fluid Mech. 46 (2014) p.97.
[19] D. Lohse and X.H. Zhang, Rev. Mod. Phys. 87 (2015) p.981.
[20] Q. Li, K.H. Luo, Q.J. Kang, Y.L. He, Q. Chen and Q. Liu, Prog. Energy Combust. Sci. 52 (2016) p.62.
[21] S. Engelnkemper, M. Wilczek, S.V. Gurevich and U. Thiele, Phys. Rev. Fluids 1 (2016) p.073901.
[22] H. Ding and P.D.M. Spelt, Phys. Rev. E 75 (2007) p.046708.
[23] R. Borcia, I.D. Borcia and M. Bestehorn, Phys. Rev. E 78 (2008) p.066307.

[24] U. Thiele and E. Knobloch, Phys. Rev. Lett. 97 (2006) p.204501.
[25] P. Beltrame, P. Hänggi and U. Thiele, EPL 86 (2009) p.24006.
[26] H. Kusumaatmaja, J. Léopoldès, A. Dupuis and J.M. Yeomans, EPL 73 (2006) p.740.
[27] D. Herde, U. Thiele, S. Herminghaus and M. Brinkmann, EPL 100 (2012) p.16002.
[28] M. Sbragaglia, L. Biferale, G. Amati, S. Varagnolo, D. Ferraro, G. Mistura and M. Pierno, Phys. Rev. E 89 (2014) p.012406.
[29] C. Semprebon and M. Brinkmann, Soft Matter 10 (2014) p.3325.
[30] C. Semprebon, S. Varagnolo, D. Filippi, L. Perlini, M. Pierno, M. Brinkmann and G. Mistura, Soft Matter 12 (2016) p.8268.
[31] N. Savva and S. Kalliadasis, J. Fluid Mech. 725 (2013) p.462.
[32] H. Kusumaatmaja and J.M. Yeomans, Langmuir 23 (2007) p.6019.
[33] S. Suzuki, A. Nakajima, K. Tanaka, M. Sakai, A. Hashimoto, N. Yoshida, Y. Kameshima and K. Okada, Appl. Surf. Sci. 254 (2008) p.1797.
[34] T. Furuta, M. Sakai, T. Isobe, S. Matsushita and A. Nakajima, Langmuir 27 (2011) p.7307.
[35] R. Ledesma-Aguilar, R. Nistal, A. Hernández-Machado and I. Pagonabarraga, Nat. Mater. 10 (2011) p.367.
[36] A. Nakajima, Y. Nakagawa, T. Furuta, M. Sakai, T. Isobe and S. Matsushita, Langmuir 29 (2013) p.9269.
[37] S. Varagnolo, D. Ferraro, P. Fantinel, M. Pierno, G. Mistura, G. Amati, L. Biferale and M. Sbragaglia, Phys. Rev. Lett. 111 (2013) p.066101.
[38] S. Varagnolo, V. Schiocchet, D. Ferraro, M. Pierno, G. Mistura, M. Sbragaglia, A. Gupta and G. Amati, Langmuir 30 (2014) p.2401.
[39] K.A. Wier, L.C. Gao and T.J. McCarthy, Langmuir 22 (2006) p.4914.
[40] A.T. Paxson and K.K. Varanasi, Nat. Commun. 4(8) (2013) p.1492.
[41] J. Buehrle, S. Herminghaus and F. Mugele, Langmuir 18 (2002) p.9771.
[42] H.P. Jansen, O. Bliznyuk, E.S. Kooij, B. Poelsema and H.J.W. Zandvliet, Langmuir 28 (2012) p.499.
[43] H.P. Jansen, K. Sotthewes, C. Ganser, H.J.W. Zandvliet, C. Teichert and E.S. Kooij, Langmuir 30 (2014) p.11574.
[44] C. Semprebon, G. Mistura, E. Orlandini, G. Bissacco, A. Segato and J.M. Yeomans, Langmuir 25 (2009) p.5619.
[45] M.J. Hancock, F. Yanagawa, Y.H. Jang, J.K. He, N.N. Kachouie, H. Kaji and A. Khademhosseini, Small 8 (2012) p.393.
[46] K.K. Varanasi, M. Hsu, N. Bhate, W.S. Yang and T. Deng, Appl. Phys. Lett. 95 (2009) p.094101.
[47] H.Y. Kim, H.J. Lee and B.H. Kang, J. Colloid Interface Sci. 247 (2002) p.372.
[48] N. Le Grand, A. Daerr and L. Limat, J. Fluid Mech. 541 (2005) p.293.
[49] S. Varagnolo, G. Mistura, M. Pierno and M. Sbragaglia, Eur. Phys. J. E 38 (2015) p.126.
[50] S. Varagnolo, D. Filippi, G. Mistura, M. Pierno and M. Sbragaglia, Soft Matter 13 (2017) p.3116.
[51] M. Morita, T. Koga, H. Otsuka and A. Takahara, Langmuir 21 (2005) p.911.
[52] F.-C. Wang and H.-A. Wu, Soft Matter 9 (2013) p.5703.
[53] J.G. Zhang, F. Müller-Plathe and F. Leroy, Langmuir 31 (2015) p.7544.
[54] H.P. Jansen, H.J.W. Zandvliet and E.S. Kooij, Int. J. Heat Mass Transf. 82 (2015) p.537.
[55] Q. Li, P. Zhou and H.J. Yan, Langmuir 32 (2016) p.9389.
[56] J. Zhao, S. Chen and Y. Liu, Appl. Surf. Sci. 400 (2017) p.515.
[57] L. Hu, Y. Huang, W.Y. Chen, X. Fu and H.B. Xie, Langmuir 32 (2016) p.11780.
[58] D.T. Mannetje, S. Ghosh, R. Lagraauw, S. Otten, A. Pit, C. Berendsen, J. Zeegers, D. van den Ende and F. Mugele, Nat. Commun. 5 (2014) p.3559.

[59] B. Chang, Q. Zhou, R.H.A. Ras, A. Shah, Z.G. Wu and K. Hjort, Appl. Phys. Lett. 108 (2016) p.154102.
[60] Y.H. Guo, D. Song, B.W. Song and H.B. Hu, Appl. Surf. Sci. 387 (2016) p.1225.
[61] Y.K. Lai, F. Pan, C. Xu, H. Fuchs and L.F. Chi, Adv. Mater. 25 (2013) p.1682.
[62] B. Balu, A.D. Berry, D.W. Hess and V. Breedveld, Lab Chip 9 (2009) p.3066.
[63] A. Ghosh, R. Ganguly, T.M. Schutzius and C.M. Megaridis, Lab Chip 14 (2014) p.1538.
[64] J.B. Boreyko, R.R. Hansen, K.R. Murphy, S. Nath, S.T. Retterer and C.P. Collier, Sci. Rep. 6 (2016) p.19131.
[65] A.R. Betz, J. Xu, H.H. Qiu and D. Attinger, Appl. Phys. Lett. 97 (2010) p.141909.
[66] Q. Meng, Y.L. Zhang, J. Li, R.G.H. Lammertink, H.S. Chen and P.A. Tsai, Sci. Rep. 6 (2016) p.26953.
[67] H.F. Bohn and W. Federle, Proc. Natl. Acad. Sci. U. S. A. 101 (2004) p.14138.
[68] U. Bauer and W. Federle, Plant Signal. Behav. 4 (2009) p.1019.
[69] N. Bjelobrk, H.L. Girard, S.B. Subramanyam, H.M. Kwon, D. Quéré and K.K. Varanasi, Phys. Rev. Fluids 1 (2016) p.063902.
[70] S. Anand, A.T. Paxson, R. Dhiman, J.D. Smith and K.K. Varanasi, ACS Nano 6 (2012) p.10122.
[71] J.S. Wexler, I. Jacobi and H.A. Stone, Phys. Rev. Lett. 114 (2015) p.168301.
[72] P. Kim, T.-S. Wong, J. Alvarenga, M.J. Kreder, W.E. Adorno-Martinez and J. Aizenberg, ACS Nano 6 (2012) p.6569.
[73] L.L. Xiao, J. Li, S. Mieszkin, A. Di Fino, A.S. Clare, M.E. Callow, J.A. Callow, M. Grunze, A. Rosenhahn and P.A. Levkin, ACS Appl. Mater. Interfaces 5 (2013) p.10074.
[74] A. Eifert, D. Paulssen, S.N. Varanakkottu, T. Baier and S. Hardt, Adv. Mater. Interfaces 1 (2014) p.1300138.
[75] J.Q. Guo, W.W. Fang, A. Welle, W.Q. Feng, I. Filpponen, O.J. Rojas and P.A. Levkin, ACS Appl. Mater. Interfaces 8 (2016) p.34115.
[76] C.Q. Wei, G.F. Zhang, Q.H. Zhang, X.L. Zhan and F.Q. Chen, ACS Appl. Mater. Interfaces 8 (2016) p.34810.
[77] S.Q. Ling, Y. Luo, L. Luan, Z.W. Wang and T.Z. Wu, Sens. Actuators B Chem. 235 (2016) p.732.
[78] J.F. Patrick, M.J. Robb, N.R. Sottos, J.S. Moore and S.R. White, Nature 540 (2016) p.363.
[79] C. Semprebon, G. McHale and H. Kusumaatmaja, Soft Matter 13 (2017) p.101.
[80] A. Carlson, G. Bellani and G. Amberg, EPL 97 (2012) p.44004.
[81] J.Z. Chen, S.M. Troian, A.A. Darhuber and S. Wagner, J. Appl. Phys. 97 (2005) p.014906.
[82] V. Pratap, N. Moumen and R.S. Subramanian, Langmuir 24 (2008) p.5185.
[83] H.A. Stone, ACS Nano 6 (2012) p.6536.
[84] M.J. Kreder, J. Alvarenga, P. Kim and J. Aizenberg, Nat. Rev. Mater. 1 (2016) p.15003.
[85] A. Carlson, P. Kim, G. Amberg and H.A. Stone, EPL 104 (2013) p.34008.
[86] A.K. Epstein, T.-S. Wong, R.A. Belisle, E.M. Boggs and J. Aizenberg, Proc. Natl. Acad. Sci. U. S. A. 109 (2012) p.13182.
[87] J. Li, T. Kleintschek, A. Rieder, Y. Cheng, T. Baumbach, U. Obst, T. Schwartz and P.A. Levkin, ACS Appl. Mater. Interfaces 5 (2013) p.6704.
[88] X. Khoo, G.A. O'Toole, S.A. Nair, B.D. Snyder, D.J. Kenan and M.W. Grinstaff, Biomaterials 31 (2010) p.9285.
[89] J.X. Chen, C. Howell, C.A. Haller, M.S. Patel, P. Ayala, K.A. Moravec, E.B. Dai, L.Y. Liu, I. Sotiri, M. Aizenberg, J. Aizenberg, E.L. Chaikof, Biomaterials 113 (2017) p.80.
[90] D.C. Leslie, D.C. Leslie, A. Waterhouse, J.B. Berthet, T.M. Valentin, A.L. Watters, A. Jain, P. Kim, B.D. Hatton, A. Nedder, K. Donovan, E.H. Super, C. Howell, C.P. Johnson, T.L. Vu, D.E. Bolgen, S. Rifai, A.R. Hansen, M. Aizenberg, M. Super, J. Aizenberg, D.E. Ingber, Nat. Biotechnol. 32 (2014) p.1134.

[91] S. Sunny, G. Cheng, D. Daniel, P. Lo, S. Ochoa, C. Howell, N. Vogel, A. Majid and J. Aizenberg, Proc. Natl. Acad. Sci. U. S. A. 113 (2016) p.11676.
[92] A.B. Tesler, P. Kim, S. Kolle, C. Howell, O. Ahanotu and J. Aizenberg, Nat. Commun. 6(10) (2015) p.8649.
[93] B.R. Solomon, K.S. Khalil and K.K. Varanasi, Langmuir 30 (2014) p.10970.
[94] Y. Liu, J.S. Wexler, C. Schönecker and H.A. Stone, Phys. Rev. Fluids 1 (2016) p.074003.
[95] J.S. Wexler, A. Grosskopf, M. Chow, Y.Y. Fan, I. Jacobi and H.A. Stone, Soft Matter 11 (2015) p.5023.
[96] X. Yao, Y. Hu, A. Grinthal, T.-S. Wong, L. Mahadevan and J. Aizenberg, Nat. Mater. 12 (2013) p.529.
[97] F. Mugele and J.C. Baret, J. Phys. Condens. Matter 17 (2005) p.R705.
[98] Z.-G. Guo, F. Zhou, J.-C. Hao, Y.-M. Liang, W.-M. Liu and W.T.S. Huck, Appl. Phys. Lett. 89 (2006) p.081911.
[99] H. Asakura, A. Nakajima, S. Munetoshi, S. Suzukia, Y. Kameshima and K. Okada, Appl. Surf. Sci. 253 (2007) p.3098.
[100] E. Bormashenko, R. Pogreb, Y. Bormashenko, A. Musin and T. Stein, Langmuir 24 (2008) p.12119.
[101] N.T. Nguyen, A. Beyzavi, K.M. Ng and X.Y. Huang, Microfluid. Nanofluidics 3 (2007) p.571.
[102] N.-T. Nguyen, G. Zhu, Y.-C. Chua, V.-N. Phan and S.-H. Tan, Langmuir 26 (2010) p.12553.
[103] N. Nam-Trung, Langmuir 29 (2013) p.13982.
[104] G. Katsikis, J.S. Cybulski and M. Prakash, Nat. Phys. 11 (2015) p.588.
[105] C. Rigoni, M. Pierno, G. Mistura, D. Talbot, R. Massart, J.C. Bacri and A. Abou-Hassan, Langmuir 32 (2016) p.7639.
[106] P. Irajizad, M. Hasnain, N. Farokhnia, S.M. Sajadi and H. Ghasemi, Nat. Commun. 7 (2016) p.13395.